Strong magneto-chiral dichroism in enantiopure chiral ferromagnets

CYRILLE TRAIN[1]*, RUXANDRA GHEORGHE[1], VOJISLAV KRSTIC[2,3], LISE-MARIE CHAMOREAU[1], NIKOLAI S. OVANESYAN[4], GEERT L. J. A. RIKKEN[3], MICHEL GRUSELLE[1]* AND MICHEL VERDAGUER[1]

[1]Laboratoire de Chimie Inorganique et Matériaux Moléculaires, UMR 7071, IFR 2769, UPMC, case 42, 4 place Jussieu, F-75252 Paris cedex 05, France
[2]Trinity College Dublin, Centre for Research on Adaptive Nanostructures and Nanodevices, Dublin 2, Ireland
[3]Laboratoire National des Champs Magnétiques Pulsés, CNRS/INSA/UPS, B.P. 14245, F-31400 Toulouse, France
[4]Institute of Problems of Chemical Physics, Russian Academy of Science, Moscow Region, 142432 Chernogolovka, Russia
*e-mail: cyrille.train@upmc.fr; michel.gruselle@upmc.fr

Published online: 17 August 2008; doi:10.1038/nmat2256

As materials science is moving towards the synthesis, the study and the processing of new materials exhibiting well-defined and complex functions, the synthesis of new multifunctional materials is one of the important challenges. One of these complex physical properties is magneto-chiral dichroism which arises, at second order, from the coexistence of spatial asymmetry and magnetization in a material. Herein we report the first measurement of strong magneto-chiral dichroism in an enantiopure chiral ferromagnet. The *ab initio* synthesis of the enantiopure chiral ferromagnet is based on an enantioselective self-assembly, where a resolved chiral quaternary ammonium cation imposes the absolute configurations of the metal centres within chromium–manganese two-dimensional oxalate layers. The ferromagnetic interaction between Cr(III) and Mn(II) ions leads to a Curie temperature of 7 K. The magneto-chiral dichroic effect is enhanced by a factor of 17 when entering into the ferromagnetic phase.

Molecular magnetism aims to control spins in molecules and molecular assemblies[1,2]. The goal is to synthesize new magnetic molecular systems with expected properties owing to the flexibility of molecular chemistry and the subtleties of supramolecular interactions between the precursors. Several challenges were overcome recently, such as molecule-based magnets at room temperature[3–5] or single-molecule magnets exhibiting exciting new quantum phenomena (slow relaxation of the magnetization, quantum tunnelling effect)[6–9]. Spin cross-over systems exhibiting bistable states at room temperature opened new prospects as well[10].

One of the most promising areas in this emerging scientific field is that of multifunctional materials where compounds combine different physical properties and functions. These functions can simply coexist[11–14] or interact with each other enabling the tuning of one of the functions by the other. Multiferroics are an important example of such interactions[15,16]. In some very rare cases a new property can arise from the coexistence in the same material of two properly designed functions. Working on such compounds is very demanding. It requires from the outset a clear understanding of the phenomenon involved to imagine the appropriate compound. A strong interaction between chemists and physicists, experimentalists and theoreticians is thus a prerequisite to design the material, master its synthesis and carry out its characterization.

The present work is devoted to the synthesis of optically active magnets in which it was theoretically predicted that the simultaneous presence of spatial asymmetry and magnetization should give rise to an optical phenomenon, called magneto-chiral dichroism, which will be briefly introduced hereafter. The fundamental optical property that distinguishes the two enantiomers of a chiral object from the racemic mixture is their ability to rotate the plane of linearly polarized light, the rotation angle being opposed for the two enantiomers. A phenomenologically similar effect named the Faraday effect is observed when a linearly polarized light interacts with a magnetized medium. In the former case, the effect is related to the breaking of parity, whereas in the latter, it is related to the breaking of time-reversal symmetry. When both symmetries are broken simultaneously, for example, for a medium possessing a magnetic moment and a spatial asymmetry, magneto-chiral dichroism becomes possible[17,18]. It can be formalized by developing the frequency-dependent dielectric tensor to first order in $\mathbf{k}$, the wave vector of light, and $\mathbf{M}$, the magnetization of the medium.

$$\varepsilon(\mathbf{k},\mathbf{M}) = \varepsilon_0 + \alpha_{\mathrm{NCD}}\mathbf{k} + \beta_{\mathrm{MCD}}\mathbf{M} + \gamma_{\mathrm{MChD}}\mathbf{k}\cdot\mathbf{M}. \qquad (1)$$

ε_0 is associated with refraction and absorption, α_{NCD} with natural circular birefringence and natural circular dichroism (NCD, Cotton effect), β_{MCD} with magnetic circular birefringence (Faraday effect) and magnetic circular dichroism and γ_{MChD} with magneto-chiral birefringence and magneto-chiral dichroism (MChD). The magneto-chiral effect is therefore a second-order effect, depending on the product $\mathbf{k}\cdot\mathbf{M}$. In contrast to the Cotton and Faraday effects, magneto-chiral effects occur when the medium interacts with non-polarized light. Such effects have been observed in the visible region on para- and dia-magnetic systems[19–22].

The time- and parity-reversal symmetry arguments underlying this magneto-chiral anisotropy are of general validity. Magneto-chiral effects related to interaction with light have indeed been observed in the luminescence of chiral complexes[19], in the

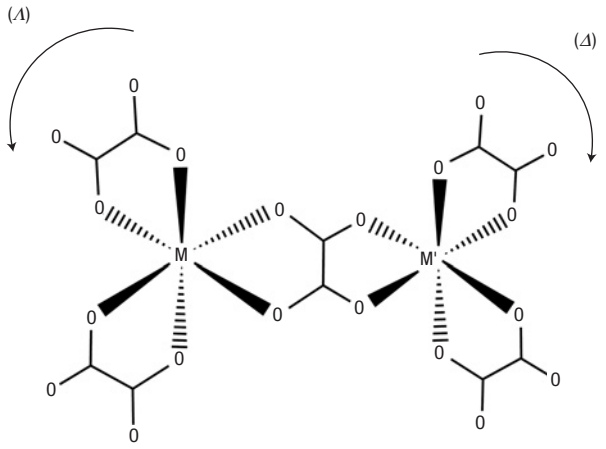

Figure 1 Weakness of the chirality in the 2D oxalate-based chiral magnets. Schematic diagram of the heterochiral $[(ox)_2M(\mu\text{-}ox)M'(ox)_2]$ moiety that builds the anionic layers.

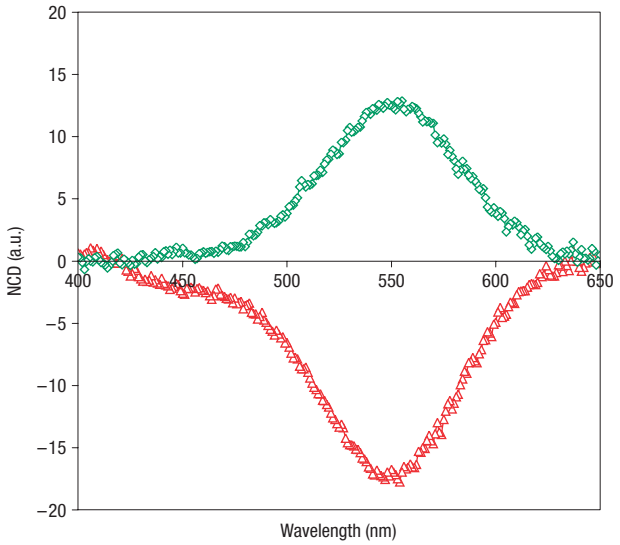

Figure 2 The counterion controls the configuration of the chromium centre. NCD for $[N(CH_3)(n\text{-}C_3H_7)_2((S)\text{-}s\text{-}C_4H_9)][(\Lambda)\text{-}Mn(\Delta)\text{-}Cr(ox)_3]$ **1** (triangles) and $[N(CH_3)(n\text{-}C_3H_7)_2((R)\text{-}s\text{-}C_4H_9)][(\Delta)\text{-}Mn(\Lambda)\text{-}Cr(ox)_3]$ **2** (diamonds).

absorption of chiral paramagnets[20] or excited states of atoms[23] and in the photolysis of chromium oxalate complexes[24,25], whereas the interplay between electron propagation, magnetic fields and chirality has been exemplified for helically structured metallic conductors[26] and chiral single-walled carbon nanotubes[27].

Testing the MChD of enantiomerically pure ferromagnets has two fundamental interests compared with the measurements carried out on para- and dia-magnetic systems[19–22]. According to equation (1), the intensity of the MChD is predicted to be proportional to the magnetization. If so, it should be enhanced in the ferromagnetic state compared with the paramagnetic one. Moreover, the bistability inherent to the existence of a magnetically ordered state can be exploited for data storage with a detection based on MChD rather than magnetic circular dichroism. Alternatively, as ferromagnetic chiral media are intrinsically magneto-electric, electrical reading/writing of the magnetic state of these media is possible, a feature that is currently widely pursued in multiferroics[16,28].

It is then necessary to define the best synthetic strategy towards enantiomerically pure ferromagnets.

Although it is not an exclusive method, the molecular approach of such multifunctional materials seems to be the most versatile one. A lot of effort has been put into obtaining molecular materials exhibiting both long-range magnetic order and chiral structures[14,29,30], although the concomitant control of both the exchange interaction, and hence the magnetic properties, and the configuration of chiral centres has rarely been demonstrated[31].

We have focused our attention on oxalate-based compounds[31–33]. The oxalate ligand $C_2O_4^{2-}$ (ox^{2-}) is indeed known for bridging two metal centres with significant exchange interaction, whereby each metal can be tris(chelated), hence exhibiting a propeller-like chiral structure of D_3 symmetry, with Δ or Λ configurations (Fig. 1). When all of the metal ions are tris(chelated) by oxalate ions, compounds of general formula $C[MM'(ox)_3]$ are obtained. The $[MM'(ox)_3]^{n-}$ ($n = 1, 2$) moiety, noted [MM'], forms either a three-dimensional (3D) or 2D coordination network. The cationic counterpart C^{n+} ($n = 1, 2$) can be exploited to control both the dimensionality of the coordination network and the absolute configurations of the chiral metal centres. The enantioselective self-assembly of 3D [MM'] networks by resolved tris(diimine)ruthenium(II) complexes have been readily tackled[34]. In such 3D systems, all of the metal centres have the same configuration as the ruthenium precursor. Unfortunately, the optical properties of the compounds are dominated by the absorption of the templating cation, preventing the observation of the MChD arising from the anionic network. Despite the fact that all of the metal centres exhibit propeller-like chirality, the enantioselective self-assembly of 2D anionic networks is much harder to rationalize and to carry out. The main reason is that within one 2D honeycomb anionic layer (Fig. 3b), adjacent metal centres have alternately Δ and Λ configurations (Fig. 1). A honeycomb cell is indeed composed of three $(ox)_2M(\mu - ox)M'(ox)_2$ heterochiral moieties. Each moiety can almost be considered as a meso dinuclear helicate[35], the chirality being non-vanishing solely because of the difference in the metal–oxygen distances for M and M′. This feature weakens the overall chirality of the structure[36].

Moreover, the chirality of one $[(\Lambda)\text{-}M(\Delta)\text{-}M']$ layer can be exactly compensated by the one of the neighbouring $[(\Delta)\text{-}M(\Lambda)\text{-}M']$ layer, leading to achiral overall structures. However, some cases of spontaneous resolution were reported[37,38] and the enantioselective self-assembly of 2D bimetallic oxalate-based materials using resolved planar chiral ferrocenic ammonium and racemic tris(oxalato)chromate(III) was demonstrated on powder samples[39]. Various tetraalkylammonium cations are known to template the formation of 2D bimetallic oxalate-based networks. They are stable during the crystallization process, but they are not chiral. To favour the formation of optically active single crystals, a robust chiral templating agent was needed. We decided to introduce a configurationally stable chiral alkyl chain on a tetraalkyl ammonium cation. The pertinence of this choice will become obvious in the following. We therefore synthesized and fully characterized the two enantiomers of methyl(1-methylpropyl)di(*n*-propyl)ammonium iodide[40].

The ability of methyl-(1-methylpropyl)di(*n*-propyl)ammonium cations $[N(CH_3)(n\text{-}C_3H_7)_2(s\text{-}C_4H_9)]^+$ to template the enantioselective formation of a bimetallic $[Mn^{II}Cr^{III}(ox)_3]^-$ anionic network was first successfully tested on powder samples starting from resolved chiral ammonium cation and

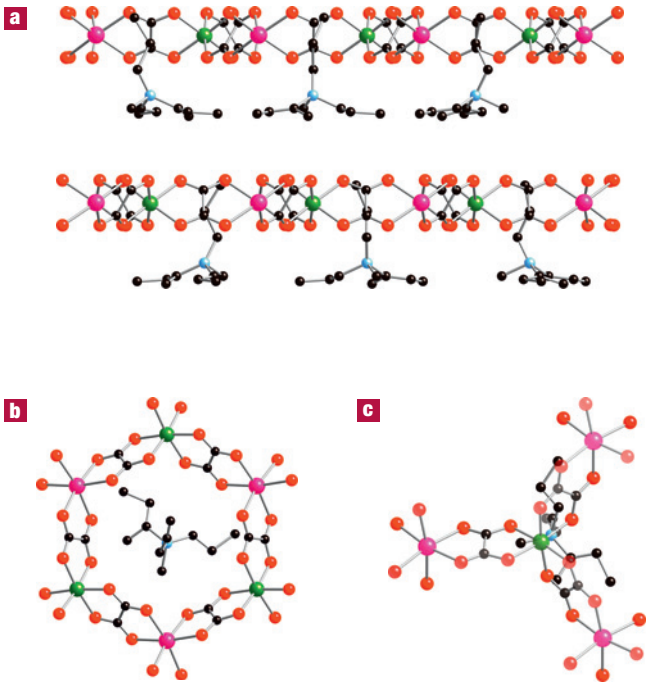

Figure 3 Crystal structure of 1. a–c, Views along the [010] (**a**), the [001] (**b**) and slightly offset [00$\bar{1}$] (**c**) directions. The alkyl chains are represented in one of their possible positions.

Table 1 Crystallographic data for compounds 1 and 2.

	1	2
System	Hexagonal	Hexagonal
Space group	$P6_3$	$P6_3$
Cell dimensions		
a, *c* (Å)	9.417(2), 16.843(1)	9.441(1),16.831(2)
Volume (Å^3)	1,293.5(4)	1,299.2(2)
Density (calculated) (Mg m^{-3})	1.395	1.389
Molecular weight	543.33	543.33
Reflections		
Collected/unique	24,084/2,506	7,113/2,394
R_{int}*	0.0505	0.0325
Theta range (°)	3.5–30.0	3.5–30.0
Completeness (%)	99.6	97.2
Data/restraints/parameters	2,506/8/91	2,394/7/91
Goodness of fit on F^2 †	1.096	1.082
$R1$ / $wR2$ ($I/2\sigma I$)‡	0.0792–0.2126	0.0794–0.2080
$R1$ / $wR2$ (all data)	0.1233/0.2350	0.1321–0.2331
Absolute structure parameter	0.24(8)	0.28(8)
Largest difference peak/hole (e Å^3)	0.777 and −0.747	0.490 and −0.912
CSD deposition number	685,531	685,532

*$R_{int} = \Sigma|F_o^2 - F_o^2(\text{mean})| / \Sigma[F_o^2]$.

† F is the structure factor.

‡ $R1 = \Sigma||F_o| - |F_c|| / \Sigma|F_o|$; $wR2 = \{\Sigma[w(F_o^2 - F_c^2)^2] / \Sigma[w(F_o^2)^2]\}^{1/2}$, with weighting scheme w given by: $w = 1/[\sigma^2(F_o)^2 + (aP)^2 + bP]$, where P is $[2F_c^2 + \text{Max}(F_o^2, 0)]/3$.

racemic tris(oxalato)chromate(III) anion, (*rac*)-$[Cr(ox)_3]^{3-}$. We present here the results for enantiopure transparent single crystals. The NCD of crushed single crystals is shown in Fig. 2. The dichroic signals obtained starting from (*S*)- and (*R*)-methyl(1-methylpropyl)di(*n*-propyl)ammonium iodide are symmetrical with respect to the wavelength axis. Because the ammonium cation does not undergo electronic transition in the 400–650 nm region[40], and the manganese absorption is very weak, the observed dichroic signal is solely due to the *d–d* transitions of the chiral $[Cr(ox)_3]$ moiety[41]. The symmetry of the two curves indicates that the resolved ammonium cation has predominantly interacted with one of the enantiomers of the tris(oxalato)chromate(III) to build optically active single crystals of $[N(CH_3)(n\text{-}C_3H_7)_2(s\text{-}C_4H_9)][MnCr(ox)_3]$ according to the following enantioselective reactions:

$$[NCH_3(C_3H_7)_2((S)\text{-}s\text{-}C_4H_9)]^+ + Mn^{2+} + (rac) - [Cr(ox)_3]^{3-}$$
$$= [NCH_3(C_3H_7)_2((S)\text{-}s\text{-}C_4H_9)][(\Lambda) - Mn(\Delta) - Cr(ox)_3]\ \mathbf{1}$$

$$[NCH_3(C_3H_7)_2((R)\text{-}s\text{-}C_4H_9)]^+ + Mn^{2+} + (rac) - [Cr(ox)_3]^{3-}$$
$$= [NCH_3(C_3H_7)_2((R)\text{-}s\text{-}C_4H_9)][(\Delta) - Mn(\Lambda) - Cr(ox)_3]\ \mathbf{2}$$

The crystal structures of the two enantiomers of $[N(CH_3)(n\text{-}C_3H_7)_2(s\text{-}C_4H_9)][MnCr(ox)_3]$ have been solved by single-crystal X-ray diffraction. The enantiomers crystallize in the chiral space group $P6_3$ with lattice parameters $a = b = 9.417(2)$ Å, $c = 16.843(1)$ Å for $[N(CH_3)(n\text{-}C_3H_7)_2((S)\text{-}s\text{-}C_4H_9)][(\Lambda)\text{-}Mn(\Delta)\text{-}Cr(ox)_3]$ **1** and $a = b = 9.441(1)$ Å, $c = 16.831(2)$ Å for $[N(CH_3)(n\text{-}C_3H_7)_2((R)\text{-}s\text{-}C_4H_9)][(\Delta)\text{-}Mn(\Lambda)\text{-}Cr(ox)_3]$ **2** (Table 1). The 2D honeycomb layers are well resolved (Fig. 3). One of the two propyl chains of the ammonium cation is located in the middle of a honeycomb cell (Fig. 3b). As often observed in the case of tetraalkyl derivatives of 2D oxalate-based compounds, there is a rotational disorder around the three-fold axis materialized by the propyl alkyl chain entering the honeycomb cell: the three other alkyl chains of the ammonium cation are statistically distributed on the three possible positions around the nitrogen atom. Because all three chains are different, this distribution blurs the electron density and prevents a good resolution of the overall structure. Therefore, the determination of the Flack parameters and hence of the absolute configurations of all of the chiral centres is not relevant[42]. Nevertheless, in the 2D bimetallic honeycomb layers, the manganese(II) and chromium(III) metal ions are clearly distinguishable from the difference in the metal–oxygen distances and it is possible to determine the absolute configuration of the metal centres. Owing to the absence of improper symmetry operation in the $P6_3$ space group, the absolute configuration of each metal ion is the same throughout the compound. It thus seems that in the 2D oxalate-based compound obtained from the $[N(CH_3)(n\text{-}C_3H_7)_2((S)\text{-}s\text{-}C_4H_9)]I$ all of the chromium(III) ions adopt the (Δ) configuration, whereas all of the manganese(II) ions adopt the (Λ) one. As expected from NCD, the opposite is observed when starting from $[N(CH_3)(n\text{-}C_3H_7)_2((R)\text{-}s\text{-}C_4H_9)]I$. The relationship between the configuration of the template cation and those of the tris(chelated) metal centres, obtained from crystallography, is in line with the NCD measurements. It is the first time that it is possible to prove from single-crystal data the enantioselective role of a template cation in the self-assembly of 2D oxalate-based compounds. The crystal structure can be further examined to understand the enantioselective activity of the ammonium cation. Figure 3b indicates that the interaction of the ammonium cation with the 'upper' layer (as defined in Fig. 3a) does not bring any enantioselectivity because (1) the alkyl chain entering the honeycomb layer is an achiral propyl chain; (2) it is located in the middle of the honeycomb cell, thus interacting

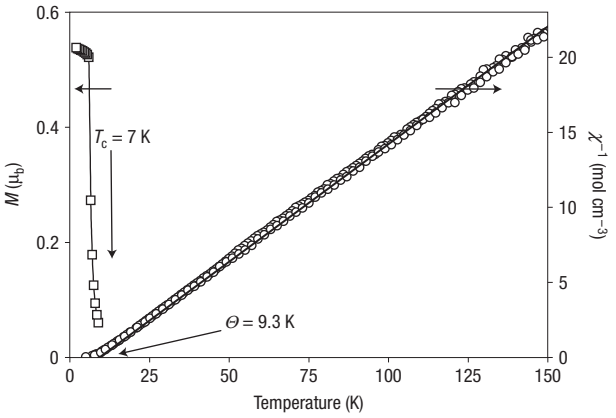

Figure 4 Magnetic properties of the chiral magnet. Thermal variations of the magnetization (left) and of the inverse molar magnetic susceptibility (right) of a single crystal of **1** with *c* parallel to the applied field.

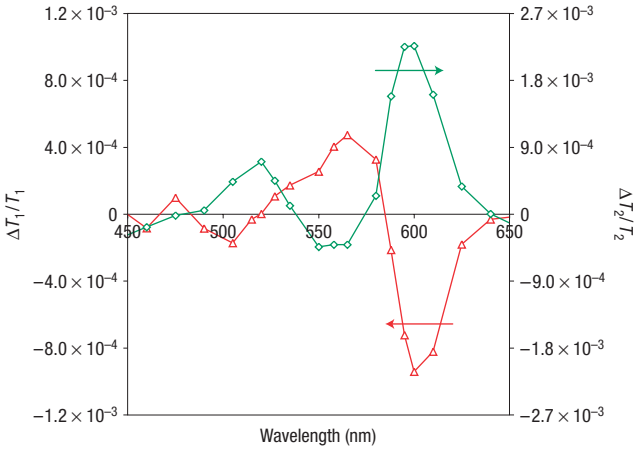

Figure 5 Inversion of the magneto-chiral dichroism with the enantiomer. Magneto-chiral dichroism measured at 4.0 K for $[N(CH_3)(n\text{-}C_3H_7)_2((S)\text{-}s\text{-}C_4H_9)][(\Lambda)\text{-}Mn(\Delta)\text{-}Cr(ox)_3]$ **1** (triangles) and $[N(CH_3)(n\text{-}C_3H_7)_2((R)\text{-}s\text{-}C_4H_9)][(\Delta)\text{-}Mn(\Lambda)\text{-}Cr(ox)_3]$ **2** (diamonds).

equivalently with the manganese(II) and chromium(III) metal centres. Conversely, the three alkyl chains of the ammonium cation are spreading over the three oxalate groups of chromium(III), which are the three blades of the chromium-centred propeller, of the underlying 2D layer (Fig. 3c). The presence of the chiral carbon atom on one chain is enough to twist the corresponding oxalate group and impose the configuration of the chromium centres. Such diastereoselective interactions are in turn responsible for the chiral conformation adopted by the in-plane butyl chains of the tetrabutylammonium ion in $NBu_4[MnCr(ox)_3]$ which is determined by the configuration of the tris(oxalato)chromate(III) moiety[43]. The diastereoselective activity of the resolved tetraalkyl cation is possible despite the weakness of the overall chirality aforementioned because the ammonium cations are located exclusively over the chromium(III) centres of the underlying layer (Fig. 3c).

The magnetic properties of the two enantiomers of $[N(CH_3)(n\text{-}C_3H_7)_2(s\text{-}C_4H_9)][MnCr(ox)_3]$ in the paramagnetic region indicate that the exchange interaction between the manganese(II) and the chromium(III) ions is ferromagnetic with a Curie–Weiss temperature of 9.3 K (Fig. 4). The compounds undergo an abrupt paramagnetic-to-ferromagnetic phase transition at $T_c = 7$ K (Fig. 4). The measurement of the isothermal magnetization at 2 K shows a rapid saturation of the magnetization and a weak remnant field. The compounds are soft ferromagnets. The magnetic properties of the two enantiomers are equivalent. All of these features are in line with those observed in the other tetraalkylammonium-containing 2D oxalate-based Mn–Cr compounds[44].

Owing to their optical activity and to their magnetic properties, the single crystals of the two enantiomers of $[N(CH_3)(n\text{-}C_3H_7)_2(s\text{-}C_4H_9)][MnCr(ox)_3]$ are optically active magnets suitable for the observation of MChD in a ferromagnetic system. In Fig. 5, the MChD signal ($\Delta T_i/T_i$, where T_i is the transmission of compound **i**) is plotted as a function of wavelength for the two enantiomers being in the ferromagnetic phase. The two enantiomers clearly show an opposite anisotropy in their optical response. This is direct experimental proof of the existence of the MChD effect in our materials. The MChD signal is significant in magnitude in the region between 570 and 640 nm and weak at other wavelengths. It is due to the *d*–*d* transitions of the chromium(III) moiety. The shape of the MChD spectrum is reminiscent of the first derivatives of the NCD signal. This feature has already been observed in $NiSO_4$ (ref. 20). We would like to point out that (1) this is the first MChD measurement in a chiral ferromagnetic phase; (2) the fact that the same centre is at the origin of the chirality and the magnetism is most probably a crucial point in the observation of an important magneto-chiral dichroic effect. Although a more detailed analysis of the MChD signal is beyond the scope of the present report, this is one of the new research fields opened by the present work.

To address the question of the change of the MChD at the transition from the paramagnetic to the ferromagnetic phase, the thermal variation of the MChD signal has been measured for **1** at a fixed wavelength, chosen at the maximum MChD signal (615 nm) (Fig. 6). In the paramagnetic phase, a weak dichroism is observed. The MChD then increases gradually when approaching the Curie temperature; the magnitude is multiplied by a factor of 17 between 11 and 3 K, when crossing the transition into the ferromagnetic phase. As shown in Fig. 6, the thermal variation of the MChD signal closely follows the thermal variation of the magnetization. As expected from equation (1), the MChD intensity is proportional to the magnetization, showing a strong enhancement at the paramagnetic-to-ferromagnetic phase transition. The importance of measuring the MChD in a ferromagnetically ordered phase to obtain a strong signal is thus clearly demonstrated.

This work presents the first magneto-chiral dichroic measurements on enantiopure single crystals of a molecule-based ferromagnet. It demonstrates the strong enhancement of the magneto-chiral dichroism in the ferromagnetic phase compared with that of the paramagnetic one. It therefore suggests that ferromagnetic chiral media could be potentially useful for data storage. Our results are also indicative that in chiral ferromagnetic conductors, large values of magneto-chiral anisotropy can be expected, which may be relevant to magneto-resistive sensors.

Two-dimensional bimetallic oxalate-bridged coordination networks enable control of both the exchange interaction between the manganese(II) and chromium(III) metal ions (hence the Curie temperature) and the absolute configurations of all the metal centres (hence the optical activity). For the latter, the control within the coordination network is guaranteed by a resolved tetraalkylammonium with a chiral carbon atom on one of the alkyl

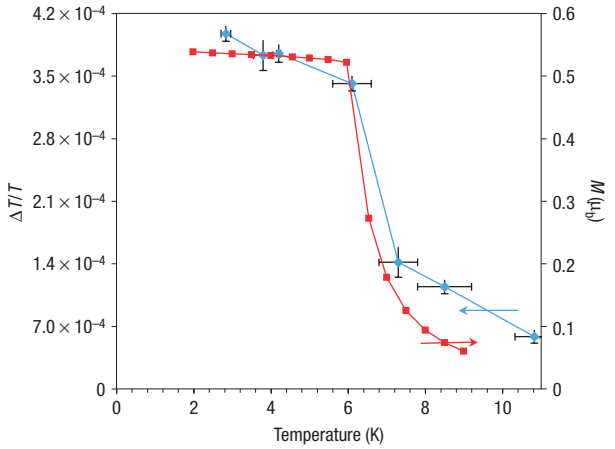

Figure 6 Enhancement of magneto-chiral dichroism at the Curie temperature of 1. Temperature dependence of the MChD effect (diamonds) measured at 615 nm and field-cooled (squares) magnetization of $[N(CH_3)(n\text{-}C_3H_7)_2((S)\text{-}s\text{-}C_4H_9)][(\Delta)\text{-}Mn(\Lambda)\text{-}Cr(ox)_3]$ **1**. The error bars on $\Delta T/T$ are calculated from the dispersion of the measurements. The uncertainty on the absolute value of the temperature increases above 4.2 K because the sample is in gaseous helium.

chains. The enantioselective self-assembly is controlled through a specific interaction between the chiral alkyl chain of the template cation and the tris(oxalato)chromate(III) moieties. The use of precursors exhibiting a weak absorbance in the whole visible range was crucial to enable the detection of the effect through optical measurements.

Our global approach based on close interactions between molecular chemists and physicists opens the way to new rationally designed optically active magnets and therefore to new studies of MChD as well as other predicted or recently experienced effects[15,16,45,46].

METHODS

SYNTHESIS

$(NH_4)_3[Cr(ox)_3]\cdot 3H_2O$, $[N(CH_3)(n\text{-}C_3H_7)_2((R)\text{-}s\text{-}C_4H_9)]I$ and $[N(CH_3)(n\text{-}C_3H_7)_2((S)\text{-}s\text{-}C_4H_9)]I$ were synthesized according to literature methods[40,47]. All other reagents were used as-received.

Single crystals of **1** and **2** were obtained either using the gel technique or the slow diffusion technique.

Gel technique: 60 mg (0.15 mmol) of $(NH_4)_3Cr(C_2O_4)_3\cdot 3H_2O$ and 37 mg (0.13 mmol) $Mn(NO_3)_2\cdot 6H_2O$ were dissolved in 3 ml of a 1:1 water/methanol mixture. 1.5 ml of $Si(OCH_3)_4$ was added to the solution. The final mixture was poured into four test tubes. After two days at room temperature, a gel is obtained. A 0.5 ml methanolic solution of $[N(CH_3)(n\text{-}C_3H_7)_2((S)\text{-}s\text{-}C_4H_9)]I$ (respectively $[N(CH_3)(n\text{-}C_3H_7)_2((R)\text{-}s\text{-}C_4H_9)]I$) (10 mg, 0.037 mmol) was added to each gel sample. After a few days, the crystallization of **1** (respectively **2**) occurs.

Slow diffusion technique: A solution of $(NH_4)_3[Cr(ox)_3]\cdot 3H_2O$ (60 mg, 0.15 mmol) in water (0.5 ml) and a solution of $Mn(NO_3)_2\cdot 6H_2O$ (37 mg, 0.13 mmol) and $[N(CH_3)(n\text{-}C_3H_7)_2((R)\text{-}s\text{-}C_4H_9)]I$ (respectively $[N(CH_3)(n\text{-}C_3H_7)_2((S)\text{-}s\text{-}C_4H_9)]I$) (40 mg, 0.15 mmol) in methanol (0.5 ml) were mixed together and stirred for 5 min. A mild precipitation takes place and the precipitate is filtered off. Single crystals are obtained after a period of 24 h, by slow diffusion of acetone into the filtrate.

NATURAL CIRCULAR DICHROISM

NCD curves were recorded using a Jasco model J-810 spectropolarimeter. 1.2 mg of product and 120 mg of KBr was ground and pressed as pellets. To enable comparison, the spectra were normalized and corrected for baseline deviation.

SINGLE-CRYSTAL X-RAY DIFFRACTION

A single crystal of each enantiomer was selected, mounted on a glass fibre and placed in a cold nitrogen gas stream. An important diffuse scattering was observed on the diffraction frames.

Intensity data were collected with graphite-monochromated Mo Kα radiation ($\lambda = 0.71073$ Å) at 250 K on a Bruker-Nonius KappaCCD diffractometer. Unit-cell parameter determinations, data collection strategies and integrations were carried out with the Nonius EVAL-14 suite of programs[48]. Multi-scan absorption correction was applied[49].

The structures were solved by direct methods using the SHELXS-97 program and refined by full-matrix least-squares methods using the SHELXL-97 software[50] and WinGX system[51]. All atoms of the $[Mn^{II}Cr^{III}(ox)_3]$ layer were refined anisotropically, whereas atoms of the ammonium cation were refined isotropically. No hydrogen atoms were introduced in the model. Geometrical restraints were applied on the cation. The methyl side chain was introduced from a Fourier difference map but its refinement needed geometrical and U_{ij}s restraints.

Crystallographic data for the structures reported here have been deposited at the Cambridge Crystallographic Data Centre with numbers CCDC 685531 and CCDC 685532. These data can be obtained free of charge from the Cambridge Crystallographic Data Centre via www.ccdc.cam.ac.uk/datarequest/cif.

MAGNETIC MEASUREMENTS

The magnetic susceptibility of single crystals of the two enantiomers was measured in a 0.1 T external field between 5 and 300 K using a Quantum Design MPMS5 superconducting quantum interference device magnetometer. The field-cooled and zero-field-cooled data were measured in a 0.01 T external field between 2 and 10 K. The susceptibility and the magnetization values were normalized with powder data, given the weak size and weight of the single crystals.

MAGNETO-CHIRAL DICHROISM

The magneto-chiral measurements were carried out on plate-like single crystals with the c axis aligned along the light propagation direction. Unpolarized light was directed onto the samples by means of optical fibres. As a light source, a commercially available mercury short-arc lamp in combination with a monochromator was used. The optical transmission T of the sample was transformed by a photomultiplier into a voltage signal. The wavelength dependence of the optical transmission of the crystals in an a.c. superconductor magnet ($B_{max} = 1.2$ T) at about 4.3 Hz was measured. The use of an a.c. magnet enabled the direct phase-sensitive measurement of the MChD as $\Delta T/T$ in the optical transmission.

Received 29 April 2008; accepted 15 July 2008; published 17 August 2008.

References

1. Kahn, O. *Molecular Magnetism* (VCH, New York, 1993).
2. Miller, J. S. & Drillon, M (eds) *Magnetism: Molecules to Materials* Vol. 1–5 (Wiley–VCH, Weinheim, 2001–2005).
3. Manriquez, J. M., Yee, G. T., McLean, R. S., Epstein, A. J. & Miller, J. S. A room-temperature molecular-organic-based magnet. *Science* **252**, 1415–1417 (1991).
4. Ferlay, S., Mallah, T., Ouahès, R., Veillet, P. & Verdaguer, M. A room-temperature organometallic magnet based on Prussian blue. *Nature* **378**, 701–703 (1995).
5. Holmes, S. M. & Girolami, G. S. Sol–gel synthesis of $KV^{II}[Cr^{III}(CN)_6]\cdot 2H_2O$: A crystalline molecule-based magnet with a magnetic ordering temperature above 100 °C. *J. Am. Chem. Soc.* **121**, 5593–5594 (1999).
6. Gatteschi, D., Caneschi, A., Pardi, L. & Sessoli, R. Large clusters of metal-ions—the transition from molecular to bulk magnets. *Science* **265**, 1054–1058 (1994).
7. Sessoli, R., Gatteschi, D., Caneschi, A. & Novak, M. A. Magnetic bistability in a metal-ion cluster. *Nature* **365**, 141–143 (1993).
8. Thomas, L. *et al.* Macroscopic quantum tunnelling of magnetization in a single crystal of nanomagnets. *Nature* **383**, 145–147 (1996).
9. Gatteschi, D., Sessoli, R. & Villain, J. *Molecular Nanomagnets* (Oxford Univ. Press, New York, 2006).
10. Gütlich, P. & Goodwin, H. A. (eds) *Spin Crossover in Transition Metal Compounds* Vol. 1–3 (Springer, Wien, 2004).
11. Kurmoo, M. *et al.* Superconducting and semiconducting magnetic charge-transfer salts—$(BEDT\text{-}TTF)_4AFe(C_2O_4)_3\cdot C_6H_5CN$ (A = H_2O, K, NH_4). *J. Am. Chem. Soc.* **117**, 12209–12217 (1995).
12. Coronado, E., Galan-Mascaros, J. R., Gomez-Garcia, C. J. & Laukhin, V. Coexistence of ferromagnetism and metallic conductivity in a molecule-based layered compound. *Nature* **408**, 447–449 (2000).
13. Ohkoshi, S. *et al.* Coexistence of ferroelectricity and ferromagnetism in a rubidium manganese hexacyanoferrate. *Angew. Chem. Int. Ed.* **46**, 3238–3241 (2007).
14. Andres, R. *et al.* Rational design of three dimensional (3D) optically active molecule-based magnets: Synthesis, structure, optical and magnetic properties of $\{[Ru(bpy)_3]^{2+}, ClO_4^-, [M^{II}Cr^{III}(ox)_3]^-\}_n$ and $\{[Ru(bpy)_2(ppy)]^+, [M^{II}Cr^{III}(ox)_3]^-\}_n$ with M^{II} = Mn, Ni; bpy = bipyridine, ppy = phenylpyridine, ox = $C_2O_4^{2-}$. X-ray Structure of

{[ΔRu(bpy)$_3$]$^{2+}$, ClO_4^-, [ΔMn^{II}ΔCr^{III}(ox)$_3$]$^-$}$_n$ and {[ΛRu(bpy)$_2$(ppy)]$^+$, [ΛMn^{II}ΛCr^{III}(ox)$_3$]$^-$}$_n$. *Inorg. Chem.* **40**, 4633–4640 (2001).
15. Spaldin, N. A. & Fiebig, M. The renaissance of magnetoelectric multiferroics. *Science* **309**, 391–392 (2005).
16. Eerenstein, W., Mathur, N. D. & Scott, J. F. Multiferroic and magnetoelectric materials. *Nature* **442**, 759–765 (2006).
17. Baranova, N. B. & Zeldovich, B. Y. Theory of a new linear magneto-refractive effect in liquids. *Mol. Phys.* **38**, 1085–1098 (1979).
18. Barron, L. D. & Vrbancich, J. Magneto-chiral birefringence and dichroism. *Mol. Phys.* **51**, 715–730 (1984).
19. Rikken, G. L. J. A. & Raupach, E. Observation of magneto-chiral dichroism. *Nature* **390**, 493–494 (1997).
20. Rikken, G. L. J. A. & Raupach, E. Pure and cascaded magnetochiral anisotropy in optical absorption. *Phys. Rev. E* **58**, 5081–5084 (1998).
21. Kleindienst, P. & Wagniere, G. H. Interferometric detection of magnetochiral birefringence. *Chem. Phys. Lett.* **288**, 89–97 (1998).
22. Vallet, M. *et al.* Observation of magnetochiral birefringence. *Phys. Rev. Lett.* **87**, 183003 (2001).
23. Sautenkov, V. A. *et al.* Electromagnetically induced magnetochiral anisotropy in a resonant medium. *Phys. Rev. Lett.* **94**, 233601 (2005).
24. Rikken, G. & Raupach, E. Enantioselective magnetochiral photochemistry. *Nature* **405**, 932–935 (2000).
25. Raupach, E., Rikken, G., Train, C. & Malezieux, B. Modelling of magneto-chiral enantioselective photochemistry. *Chem. Phys.* **261**, 373–380 (2000).
26. Rikken, G. L. J. A., Fölling, J. & Wyder, P. Electrical magnetochiral anisotropy. *Phys. Rev. Lett.* **87**, 236602 (2001).
27. Krstic, V., Roth, S., Burghard, M., Kern, K. & Rikken, G. Magneto-chiral anisotropy in charge transport through single-walled carbon nanotubes. *J. Chem. Phys.* **117** , 11315–11319 (2002).
28. Kimura, T., Sekio, Y., Nakamura, H., Siegrist, T. & Ramirez, A. P. Cupric oxide as an induced-multiferroic with high-T_c. *Nature Mater.* **7**, 291–294 (2008).
29. Coronado, E. *et al.* Design of chiral magnets: cyanide-bridged bimetallic assemblies based on cyclohexane-1,2-diamine. *Polyhedron* **22**, 2435–2440 (2003).
30. Inoue, K., Kikuchi, K., Ohba, M. & Okawa, H. Structure and magnetic properties of a chiral two-dimensional ferrimagnet with T_c of 38 K. *Angew. Chem. Int. Ed.* **42**, 4810–4813 (2003).
31. Gruselle, M., Train, C., Boubekeur, K., Gredin, P. & Ovanesyan, N. Enantioselective self-assembly of chiral bimetallic oxalate-based networks. *Coord. Chem. Rev.* **250**, 2491–2500 (2006).
32. Pilkington, M. & Decurtins, S. in *Magnetism: Molecules to Materials II* (eds Miller, J. S. & Drillon, M.) 339–356 (Wiley–VCH, Weinheim, 2001).
33. Clement, R., Decurtins, S., Gruselle, M. & Train, C. Polyfunctional 2-(2D) and 3-(3D) dimensional oxalate bridged bimetallic magnets. *Monatsh. Chem.* **134**, 117–135 (2003).
34. Andres, R., Gruselle, M., Malezieux, B., Verdaguer, M. & Vaissermann, J. Enantioselective synthesis of optically active polymeric homo- and bimetallic oxalate-bridged networks [M$_2$(ox)$_3$]$_n$. *Inorg. Chem.* **38**, 4637–4646 (1999).
35. Provent, C. & Williams, A. F. in *Transition Metals in Supramolecular Chemistry* (ed. Sauvage, J.-P.) 135–191 (Wiley, Chichester, 1999).
36. Alvarez, S., Alemany, P. & Avnir, D. Continuous chirality measures in transition metal chemistry. *Chem. Soc. Rev.* **34**, 313–326 (2005).
37. Carling, S. G. *et al.* Crystal structure and magnetic properties of the layer ferrimagnet N(n-C$_6$H$_{11}$)$_4$Mn^{II}Fe^{III}(C$_2$O$_4$)$_3$. *J. Chem. Soc. Dalton Trans.* 1839–1843 (1996).
38. Bénard, S. *et al.* Structure and NLO properties of layered bimetallic oxalato-bridged ferromagnetic networks containing stilbazolium-shaped chromophores. *J. Am. Chem. Soc.* **122**, 9444–9454 (2000).
39. Gruselle, M. *et al.* Enantioselective self-assembly of bimetallic [Mn^{II}(Δ)-Cr^{III}(C$_2$O$_4$)$_3$]$^-$ and [Mn^{II}(Λ)-Cr^{III}(C$_2$O$_4$)$_3$]$^-$ layered anionic networks templated by the optically active (Rp)- and (Sp)-[1-CH$_2$N(n-C$_5$H$_7$)$_3$-2-CH$_3$-C$_5$H$_3$Fe-C$_5$H$_5$]$^+$ cations. *Chem. Eur. J.* **10**, 4763–4769 (2004).
40. Gheorghe, R. *et al.* Enantiomerically pure quaternary ammonium salts with a chiral alkyl chain N(CH$_3$)(*n*-C$_3$H$_7$)$_2$(*s*-C$_4$H$_9$)I: Synthesis and physical studies. *Chirality* (2008, in the press).
41. Gillard, R. D., Shepherd, D. J. & Tarr, D. A. Optically-active coordination-compounds.38. Circular-dichroism of labile trioxalatometallate(III) complexes. *J. Chem. Soc. Dalton Trans.* 594–599 (1976).
42. Flack, H. D. & Bernardinelli, G. Reporting and evaluating absolute-structure and absolute-configuration determinations. *J. Appl. Cryst.* **33**, 1143–1148 (2000).
43. Atovmyan, L. O. *et al.* Structural, magnetic and Moessbauer studies of the molecular ferromagnet compounds NBu$_4$[MCr(C$_2$O$_4$)$_3$] (Bu = (CH$_2$)$_3$CH$_3$, M = Mn, Fe). *Synth. Metals* **71**, 1809–1810 (1995).
44. Tamaki, H. *et al.* Design of metal-complex magnets. Syntheses and magnetic properties of mixed-metal assemblies {NBu$_4$[MCr(C$_2$O$_4$)$_3$]}$_x$ (NBu$_4^+$ = tetra(n-butyl)ammonium ion; ox^{2-} = oxalate ion; M = Mn^{2+}, Fe^{2+}, Co^{2+}, Ni^{2+}, Cu^{2+}, Zn^{2+}). *J. Am. Chem. Soc.* **114**, 6974–6979 (1992).
45. Jung, J. H. *et al.* Optical magnetoelectric effect in the polar $GaFeO_3$ ferrimagnet. *Phys. Rev. Lett.* **93**, 037403 (2004).
46. Sawada, K. & Nagaosa, N. Optical magnetoelectric effect in multiferroic materials: Evidence for a Lorentz force acting on a ray of light. *Phys. Rev. Lett.* **95**, 237402 (2005).
47. Bailar, J. C. & Jones, E. M. Synthesis of tris(oxalato)metalate(III) potassium and salts. *Inorg. Synth.* **1**, 37–40 (1939).
48. Duisenberg, A. J. M., Kroon-Batenburg, L. M. J. & Schreurs, A. M. M. An intensity evaluation method: EVAL-14. *J. Appl. Crystallogr.* **36**, 220–229 (2003).
49. Blessing, R. H. An empirical correction for absorption anisotropy. *Acta Crystallogr. A* **51**, 33–38 (1995).
50. Sheldrick, G. M. A short history of SHELX. *Acta Crystallogr. A* **64**, 112–122 (2008).
51. Farrugia, L. J. WinGX suite for small-molecule single-crystal crystallography. *J. Appl. Crystallogr.* **32**, 837–838 (1999).

Acknowledgements

This work was supported by the UPMC, CNRS and Russian Academy of Sciences. The authors acknowledge financial support from Deutsche Forschungsgemeinschaft (RI 1027 for instrumentation and SPP 1137 for the grant of R.G.), CNRS/RAS Joint Research Program (project No. 16332) and the RFBR grant No. 05-03-33026. Discussions with K. Boubekeur about the crystallographic determination were particularly useful.

Author contributions

C.T. proposed the appropriate chiral ammonium, undertook the magnetic measurements, took part in the MChD measurements and coordinated the whole work. R.G. carried out the synthesis and single-crystal growth. V.K. carried out the MChD measurements. L.M.C. recorded the crystallographic data and solved the structure. N.S.O. took part in the analysis of the magnetic and structural data. G.L.J.A.R. conceived and built the cryostat and the MChD measurement device and supervised the MChD measurements. M.G. was in charge of the synthetic part of the project from the beginning and supervised daily the synthetic work of R.G. M.V. launched the chiral magnets project and took part in the MChD measurements.

Author information

Reprints and permission information is available online at http://npg.nature.com/reprintsandpermissions. Correspondence and requests for materials should be addressed to C.T. or M.G.